

# From RGB to Spectrum for Natural Scenes via Manifold-based Mapping

Yan Jia<sup>1</sup>, Yinqiang Zheng<sup>2</sup>, Lin Gu<sup>2</sup>, Art Subpa-Asa<sup>3</sup>, Antony Lam<sup>4</sup>, Yoichi Sato<sup>5</sup>, Imari Sato<sup>2</sup>

<sup>1</sup>RWTH Aachen University, Germany    <sup>2</sup>National Institute of Informatics, Japan

<sup>3</sup>Tokyo Institute of Technology, Japan    <sup>4</sup>Saitama University, Japan    <sup>5</sup>University of Tokyo, Japan

## Abstract

*Spectral analysis of natural scenes can provide much more detailed information about the scene than an ordinary RGB camera. The richer information provided by hyperspectral images has been beneficial to numerous applications, such as understanding natural environmental changes and classifying plants and soils in agriculture based on their spectral properties. In this paper, we present an efficient manifold learning based method for accurately reconstructing a hyperspectral image from a single RGB image captured by a commercial camera with known spectral response. By applying a nonlinear dimensionality reduction technique to a large set of natural spectra, we show that the spectra of natural scenes lie on an intrinsically low dimensional manifold. This allows us to map an RGB vector to its corresponding hyperspectral vector accurately via our proposed novel manifold-based reconstruction pipeline. Experiments using both synthesized RGB images using hyperspectral datasets and real world data demonstrate our method outperforms the state-of-the-art.*

## 1. Introduction

Spectral analysis of natural scenes can provide much more detailed information about the scene than an ordinary RGB camera. The richer information provided by hyperspectral imaging has been beneficial to numerous applications in agriculture and land health surveillance, such as understanding natural environmental changes and classifying plants and soils based on their spectral properties. Most general approaches to imaging the spectra of a scene capture narrowband hyperspectral image stacks at consecutive wavelengths. A number of optical elements are required to achieve this task, and commercially available hyperspectral imaging cameras are often expensive and tend to suffer from spatial, spectral, and temporal resolution issues.

The goal of this work is providing a cost-efficient solution for hyperspectral imaging that can reconstruct the spectra of a natural scene from a single RGB image captured by a camera with known spectral response. Obviously, the transformation from RGB to spectra is a three-to-many mapping and thus cannot be unambiguously determined unless some prior knowledge about the transformation is introduced. Indeed, there is existing work that establishes such priors. In the field of spectral reflectance recovery, researchers have examined large sets of spectral reflectance distributions and their corresponding RGB vectors in order to learn how to map from RGB to spectra. Examples include radial basis function (RBF) network mapping [23] and constrained sparse coding [2]. More recently, Arad and Shahar used a large sparse dictionary of spectra and corresponding RGB projections that could then be used as a basis to map RGB vectors to spectra [3]. However, existing approaches directly operate on the RGB space without explicitly exploring the data structure of spectral information, thus requiring a large amount of data for training.

We propose a two-step manifold-based mapping and reconstruction pipeline to reconstruct the spectra from a single RGB image. We start by investigating the intrinsic dimensionality of the spectra of natural scenes. By applying a nonlinear dimensionality reduction technique to a large set of natural spectra, we show that the spectra of natural scenes lie on an intrinsically low dimensional manifold. Based on the derived manifold, we learn an accurate nonlinear mapping from RGB to the 3D embedding. By doing so, we reduce the problem of the three-to-many mapping (RGB to spectrum) to a well-conditioned and compact three-to-three mapping (RGB to 3D embedding of spectra). Compared to previous proposed approaches that aim to solve the three-to-many mapping directly, the three-to-three mapping allows us to train a more accurate model. After mapping to the 3D embedding, the original spectrum can be recovered using a manifold-based reconstruction technique.

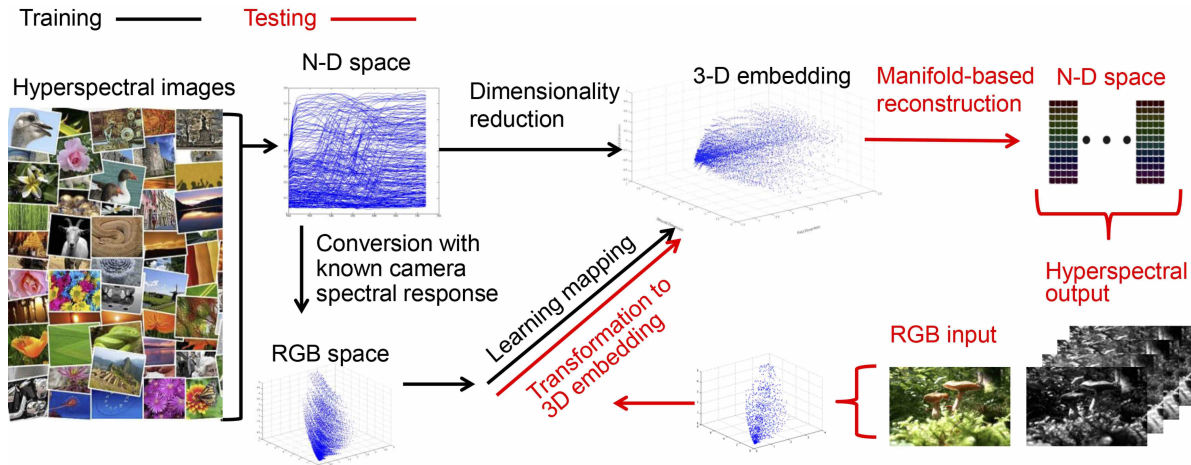


Figure 1: Scene spectra are recovered from RGB observation through our proposed nonlinear manifold learning and reconstruction technique based on pre-learned mapping between training RGB values and their corresponding 3D embedding.

Our major contributions are summarized as follows:

- This paper presents a cost-efficient solution for hyperspectral imaging that requires only a single RGB image of a scene captured by a camera with known spectral response.
- We investigate the intrinsic dimensionality of the spectra of natural scenes by a nonlinear dimensionality reduction technique. We find that natural scene spectra approximately reside in a 3D embedded space.
- We propose a two-step manifold-based mapping and reconstruction pipeline that avoids solving the difficult three-to-many mapping problem. Namely, we transform any given RGB vector to a 3D point in the embedding of natural spectra. From there, the corresponding spectrum is recovered using a manifold-based reconstruction technique.

## 2. Related Work

Hyperspectral imaging has proven beneficial to many applications in agriculture, remote sensing, medical diagnosis, and others. As a result, there is a large body of work on hyperspectral imaging of scenes. Approaches such as push broom scanning a spatial line or switching narrow bandpass filters in front a grayscale camera [14] for each wavelength of interest are in common use. However, these imaging approaches are slow. In response to issues with speed, snapshot hyperspectral cameras have been developed [5, 10, 13, 27]. Despite the better speed, spectral resolution is typically sacrificed. In addition, all hyperspectral cameras usually have lower spatial resolution than typical RGB cameras. Thus there have also been efforts at combining hyperspectral and RGB cameras together [1, 6, 17, 12]. In

these setups, the RGB and hyperspectral camera are made to share a common field-of-view. The spatial and spectral information from both cameras are then combined to form a high-spatial resolution, hyperspectral image. All the different kinds of hyperspectral camera setups have their own pros and cons but a common drawback is that they are often expensive and not as accessible.

Thus there have been attempts to use conventional RGB cameras to capture the spectral information of a scene, in particular, the spectral reflectance of scene points. One general approach is to use active lighting [8, 15, 19, 24] by taking advantage of the well-known statistical property that spectral reflectance seen in natural scenes mostly exists in a low-dimensional linear subspace of the high-dimensional space of arbitrary spectral reflectance [9, 21, 25, 16, 22, 4]. In these approaches using active lighting, an RGB or grayscale camera is used to capture multiple images of a scene under controlled lighting. By carefully defining the light spectra used and knowing the camera spectral response, it is possible to recover the spectral reflectance of surface points. However, this does not work in outdoor settings or in a number of everyday situations where the illumination cannot be controlled. Also, sometimes the lighting condition of a given environment is of interest.

For more widespread applicability, passive imaging approaches are preferred. In addition, it would be good to be able to capture hyperspectral images without any specialized equipment. Thus some researchers have proposed approaches for reconstructing the hyperspectral image of a scene from a single RGB image by learning a mapping from RGB vectors to spectra using a large set of spectral reflectance distributions and their corresponding RGBs. Nguyen et al. proposed to learn the transformation from white balanced RGB values to illumination-free reflectance

spectra based on a radial basis function (RBF) network mapping [23]. Antonio proposed to learn the prototype set from the database based on a constrained sparse coding approach and use it for illumination-free spectral recovery [2]. More recently, Arad and Ben-Shahar created a large database of natural scene hyperspectral images and derived a sparse dictionary of hyperspectral signatures and their RGB projections. The dictionary and corresponding RGB projections could then be used as a basis to estimate the spectrum of any given RGB vector [3]. These approaches tackled a difficult inverse problem involving a three-to-many mapping, and thus priors needed to be established for effective learning. This is typically accomplished by using large amounts of training data.

Our method is different from previously proposed ones in the sense that we avoid directly solving a three-to-many mapping of the RGB vector to spectrum. Specifically, we propose a two-step manifold-based mapping and reconstruction pipeline by considering the intrinsic dimensionality of natural scene spectra. This leads to a formulation of the problem where we can map an RGB vector to a spectrum as a well-conditioned three-to-three mapping (RGB to 3D embedded spectra). The original spectra can then be recovered via low-dimensional manifold reconstruction.

### 3. Spectral Reconstruction of Natural Spectra via Manifold-based Nonlinear Mapping

This paper focuses on recovering the spectra of outdoor scenes under daylight illumination from a single RGB image captured by a camera with known spectral response. Fig. 1 shows the flow of our method for spectral reconstruction. Our method consists of training and testing stages, which are indicated using black and red arrows, respectively in the figure.

In the training stage, given a large set of natural spectra, we first investigate the intrinsic dimensionality of natural scene spectra using a nonlinear dimensionality reduction technique (Sec. 3.1). Specifically, we show that the spectra of natural scenes lie on an intrinsically low dimensional manifold. At the same time, for each spectrum in the database, a corresponding RGB vector is computed based on the spectral responses of the RGB camera. Once the set of RGB and spectrum pairs is prepared, a transformation from RGB vectors to their corresponding three dimensional embedded spectra is learned (Sec. 3.2).

In the testing stage, we can first transform an input RGB vector into the three dimensional embedding using the learned transformation. Once the RGB vector is transformed into a 3D point in the embedding, the original spectrum is reconstructed from a manifold-based reconstruction technique (Sec. 3.3). In the following, we describe each step of our method in detail.

### 3.1. Analyzing Dimensionality of Natural Scene Spectra

It has been widely examined and accepted that the reflectance spectra of natural objects lie in a low-dimensional subspace or manifold [9, 21, 25, 16, 22, 4]. This leads us to speculate that spectra of natural scenes are intrinsically low-dimensional as well, since the radiance of a scene point is a compound of the illumination and surface reflectance [2, 23]. Specifically, by assuming that the scene point is diffuse, its radiance  $i(\lambda)$  can be roughly expressed by

$$i(\lambda) = l(\lambda)r(\lambda), \quad (1)$$

in which  $l(\lambda)$  and  $r(\lambda)$  denote the illumination and reflectance intensity at wavelength  $\lambda$ . By stacking all spectra of a hyperspectral image into a matrix  $I$ , we obtain

$$I = \begin{bmatrix} i_1(\lambda_1) & \cdots & i_M(\lambda_1) \\ \cdots & \cdots & \cdots \\ i_1(\lambda_N) & \cdots & i_M(\lambda_N) \end{bmatrix} = \underbrace{\begin{bmatrix} l(\lambda_1) & 0 & 0 \\ 0 & \cdots & 0 \\ 0 & 0 & l(\lambda_N) \end{bmatrix}}_L \underbrace{\begin{bmatrix} r_1(\lambda_1) & \cdots & r_M(\lambda_1) \\ \cdots & \cdots & \cdots \\ r_1(\lambda_N) & \cdots & r_M(\lambda_N) \end{bmatrix}}_R, \quad (2)$$

in which  $M$  and  $N$  denote the number of pixels and the number of bands, respectively. From the viewpoint of linear algebra, the rank of  $I$  should be no greater than that of  $R$ , which is low-dimensional for natural reflectance materials.

For real natural scenes, the model in Equation 2 may not hold accurately because of complex surface reflectance properties. Therefore, we follow a widely used criterion [26], the residual variance of dimensionality reduction, to determine the intrinsic dimensionality of natural scene spectra. At first, Isometric Feature Mapping (Isomap) [26], a nonlinear dimensionality reduction method, was applied on the natural scene spectra to embed them into a low dimensional space. Isomap estimates the intrinsic geometry of a data manifold by examining a neighborhood graph of the data points constructed in high-dimensional space. This neighborhood graph is used for computing pairwise geodesic distances between two points measured over the manifold. Once a matrix containing the geodesic distances between all data points is obtained, classical MDS is applied to this matrix to find a low-dimensional embedding of the data points such that the estimated intrinsic geometry is best preserved through dimensionality reduction. By following the procedure of [26], we calculate the residual variance  $1 - R^2(D_m, D_{gt})$ , where  $D_m$  is the matrix of Euclidean distances of the low dimensional embedding, while  $D_{gt}$  is the graph distance matrix of the input data.  $R$  is the standard correlation coefficient between  $D_m$  and  $D_{gt}$ . The intrinsic degrees of freedom is then observed at the "elbow"

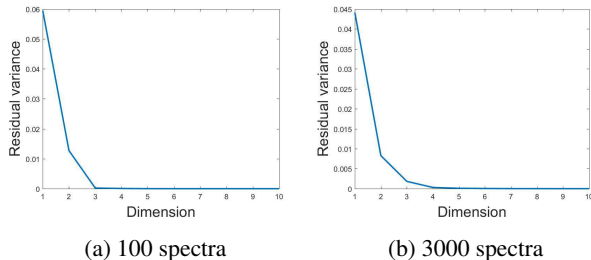


Figure 2: The residual variance of Isomap on representative spectra from [3]. (a) 100 representative spectra from [3], (b) 3000 representative spectra from [3].

where the curves of residual variance stop decreasing significantly with the added dimensions as illustrated in Fig. 2. We refer to Tenenbaum *et al.* [26] for details.

With this criterion, we conducted a dimensionality analysis of spectra of natural scenes on the natural hyperspectral image database<sup>1</sup> provided by Arad and Ben-Shahar [3], which is the largest spectral database for natural scenes available today. In Fig. 2, we report the residual variance on (a) 100 main representative spectra picked up by k-means from [3] and (b) another 3000 representative spectra collection from [3]. This figure shows that Isomap detects the dimensionality as **three** where the residual variance is almost zero on both 100 representative spectra and 3000 spectra. This observation echoes the existing research on the sparsity of natural scenes. However, it worth noting that the spectral sampling resolution of this dataset is 10 nm, which has left out finer spectral details.

### 3.2. Conversion from RGB to 3D Embedding of Scene Spectra

After finding the low dimensional embedding of natural scene spectra, a mapping  $f$  is learned between RGB vectors and their corresponding 3D embedded natural scene spectra as:  $f : \mathbb{R}^3 \rightarrow \mathbb{R}^3$ . Through experimental validation, we employ the compact neural network (a radial basis function with 10 hidden neurons) to learn a nonlinear transformation  $f$  between RGB vectors and their corresponding 3D embedded spectra. We used the Levenberg-Marquardt training algorithm [18, 11], which minimizes the following equation:

$$\hat{\beta} = \arg \min_{\beta} \sum_{i=1}^m [y_i - f(p_i, \beta)]^2, \quad (3)$$

where each  $p, y \in \mathbb{R}^3$  is a pair of RGB vector and corresponding 3D embedded spectrum in the training set, and  $\beta$  is the parameter to be found for the model  $f(p, \beta)$  to fit the training pairs  $(p_i, y_i)$ , so that the sum of the squares of the deviations is minimized.

<sup>1</sup><http://icvl.cs.bgu.ac.il/hyperspectral/>

### 3.3. Spectra Reconstruction from 3D Embedding

The main focus of dimensionality reduction techniques is how to efficiently reduce the dimensionality of high dimensional inputs by revealing meaningful structure hidden in the data. Many nonlinear dimensionality reduction techniques thus rarely consider the inverse problem of reconstructing original data from the derived low dimensional embeddings. In order to reconstruct original spectra from its 3D embedding, we employ a dictionary learning based technique [29] that learns dictionary pairs for high and low dimensional spaces and uses their relationship for reconstruction of high dimensional data from a point in the embedding.

Let  $x_i \in \mathbb{R}^{N \times 1}$  denote a high dimensional spectrum and  $g(x_i) = y_i \in \mathbb{R}^{3 \times 1}$  denote the 3D embedding of the spectrum. Then we wish to find a high dimensional dictionary  $D_H = [d_1, \dots, d_K]$  and coding scalars  $c_i = [c_{1i}, c_{2i}, \dots, c_{Ki}]^T$  such that these two functions are minimized<sup>2</sup>:

$$\sum_{i=1}^M \left\| g(x_i) - \sum_{j=1}^K c_{ji} g(d_j) \right\|^2, \sum_{i=1}^M \left\| x_i - \sum_{j=1}^K c_{ji} d_j \right\|^2 \quad (4)$$

for all  $M$  spectra in our training dataset. By doing so, we are essentially finding a common coding between the 3D embedding and high dimensional space of the spectra. Then given the estimated coding  $C = [c_1, c_2, \dots, c_M]$  and all embeddings  $Y = \{y_1, \dots, y_M\}$ , we can determine the 3D embedding dictionary  $D_L$  by:

$$\min_{D_L} \|Y - D_L C\|_F^2. \quad (5)$$

For a new point in the low dimensional space  $y_t$ , we can compute its coding  $C_T$  over the low dimensional dictionary  $D_L$ . Then the high dimensional data of  $y_T$  can be reconstructed as  $x_T = D_H C_T$ .

## 4. Experiment Results

In this section, we evaluate our manifold based mapping on both public hyperspectral datasets [3, 28, 7] and real world images. The dataset in [3] comprises of 200 images, which is by far the most comprehensive natural hyperspectral database. Similarly, the Harvard Outdoor Dataset [7] consists of 50 outdoor images in daylight illumination. Though our method is based on low dimension assumptions about natural spectra, the comparison on the indoor dataset CAVE [28], which has 64 images of indoor scenarios, is also conducted. The three datasets cover complex scenarios including various materials, multiple illuminations and shadows. We use the learned mapping to recover the spectra

<sup>2</sup>See [29] for details.

Datasets	[3]	Harvard [7]	CAVE [28]
Our	3.60 ± 1.23	6.77 ± 3.43	13.41 ± 10.94
[23]	16.31 ± 4.05	22.27 ± 8.51	16.17 ± 19.61
[3]	6.54 ± 1.71	19.30 ± 6.86	25.36 ± 20.59

Table 1: The average and variance of NRMSD (%) of reconstruction on the hyperspectral databases [3, 7, 28].

of simulated and real RGB images. We quantitatively compare our method with [23] and [3]. To further validate the robustness of our method, we also evaluate the performance under different parameter settings.

#### 4.1. Training Data and Parameter Settings

In default, for each database, we randomly split half of the images as training set and the rest for testing. To avoid over-fitting, we also report the performance on a smaller training set in Section 4.3. Since some of these images contain large dark background areas, naive acquisition of our hyperspectral training set by randomly sampling these images is likely to produce a biased result where the genuine hyperspectral information is severely underrepresented. To resolve this issue, we randomly pick 1000 spectra from each image in the training set, and use the K-means algorithm [20] to collect the most dominant  $W$  spectra for the training set. We set  $W$  to be 100 in all our experiments.

The camera spectral response function we used here to synthesize RGB values is from the Canon 5D Mark II. A radial basis function neural network with 10 hidden neurons is used to map the RGB values to the embedding of dimensionality of 3 unless explicitly stated otherwise. To verify the quantitative accuracy for spectral reflectance reconstruction, we use the normalized root mean square deviation (NRMSD) as our metric, calculated by  $\epsilon_{r(x)} = \sqrt{\frac{\sum_{\lambda} (r(\lambda, x) - r_{gt}(\lambda, x))^2}{N\bar{r}(x)}}$ , where  $r(\lambda, x)$  and  $r_{gt}(\lambda, x)$  are the reconstructed and actual spectral reflectances of the pixel  $x$ ,  $\bar{r}(x)$  is the average value across wavelengths for spectrum  $x$ .  $N$  is the number of bands in the pixel. NRMSD normalizes each ground truth spectrum to avoid bias toward strong signals.

#### 4.2. Evaluation on Hyperspectral Datasets

We first compare the spectra reconstruction performance on the three aforementioned hyperspectral image databases [3, 28, 7]. The trained nonlinear mapping is used to recover hyperspectral images from the RGB images in the testing sets. In Table 1, we present the quantitative comparison of our method, [23] and [3] for the whole testing sets. This table shows our method outperforms the alternatives in terms of spectra reconstruction accuracy. We note that, though CAVE is an indoor dataset that does not strictly follow our

assumptions about natural spectra, our method still manages to achieve superior performance over alternative methods. We also present Fig. 3, which shows the recovered spectra for three randomly selected pixels from three test images. We can see that the performance of our method is consistently better than that of [23] and [3].

To examine the spatial consistency of the recovered hyperspectral images, we also present some images at seven different wavelengths as exemplary images in Fig. 4. We can observe that the recovered images from our method are consistently accurate across the wavelength axis, irrespective of the scene materials. Our method performs particularly well on the 460nm and 500nm bands where the alternatives often encounter much error. We also note that the performance of all methods deteriorate at the 420nm band. The reason is that the camera response is very weak at the blue end, and the inaccuracy in mapping has a critical influence on the recovery results.

In Fig. 5, we also show the typical scenarios where our method gives best and worse performance in terms of NRMSD between the reconstructed spectra and the ground truth. Our method works best in the scenarios where artificial materials such as buildings occupy much of the image. It might be due to the fact that artificial materials have similar chemical compositions and thus exhibit similar spectra. In contrast, our performance fails when the image is over/under exposed, like in the first image of the second row. Natural objects such as plants also present challenges. However, especially among challenging scenarios, our method consistently generates better reconstruction compared to the alternatives.

#### 4.3. Analysis on Parameter Sensitivities

To demonstrate the robustness of our algorithm, we also analyze the sensitivity of our method to the size of the training set, the manifold dimensionality and the swap of camera response functions. When trained with only 60 images in [3], our method still achieves a satisfactory average NRMSD 4.18%, compared to 3.60% that is trained with 100 images as reported in Section 4.2.

As analyzed in Section 3.1, we observed that the dimensionality of three is sufficient in representing the natural spectra. To evaluate this observation in our system, we calculate the reconstruction errors on [3], when mapping the RGB values to the embedding of dimensionality of 4 and 5, rather than 3 used in all other experiments. We found that the average NRMSD increases as the dimensionality goes up, which is 3.60% for 3 dimensions, 3.94% for 4 dimensions and 4.01% for 5 dimensions. Adding more dimensions seems to be detrimental to accuracy, because it might introduce noises into the RGB to spectrum learning process.

Our experiments also show the robustness over various camera spectral response functions. For the dataset [3], the

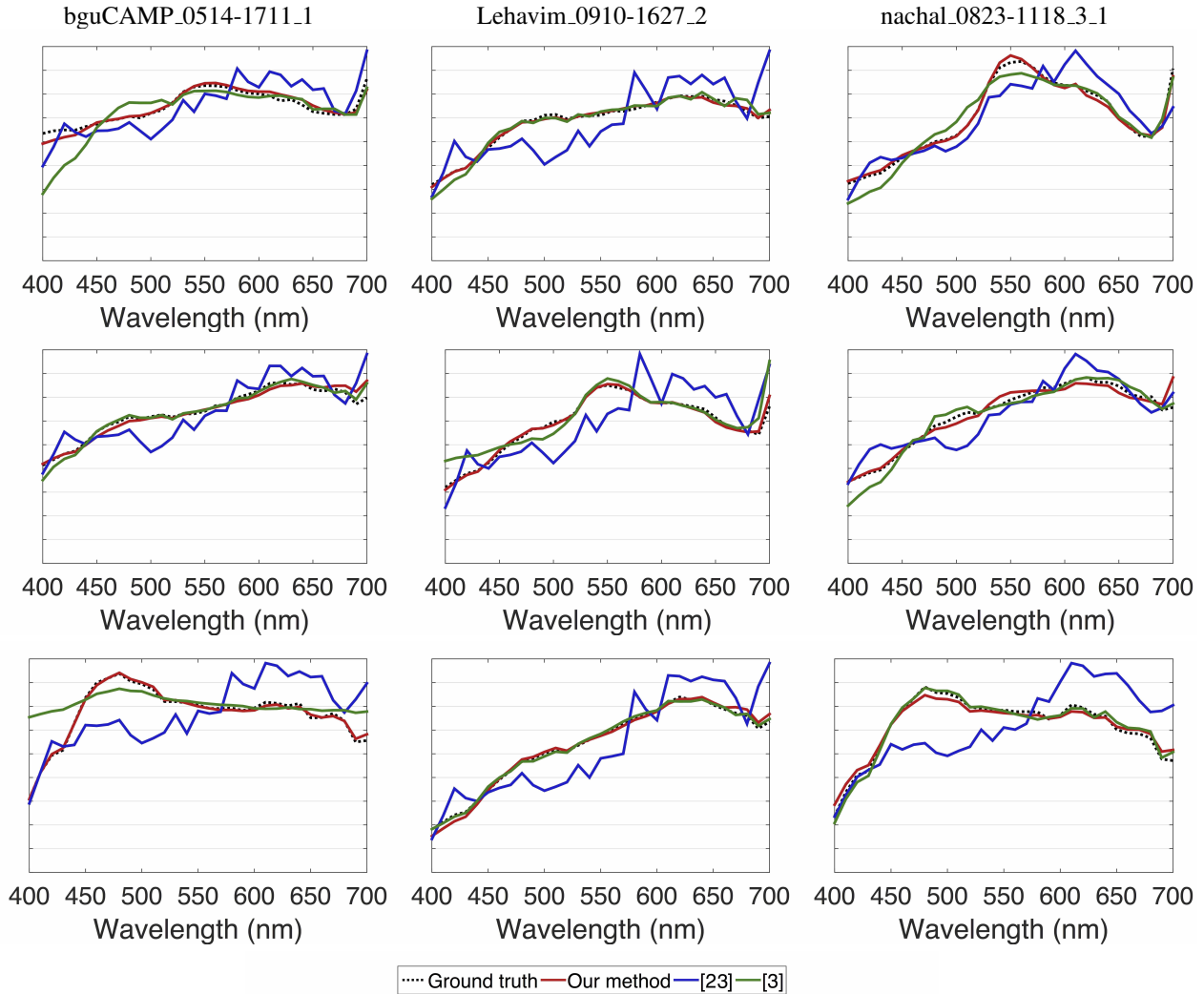


Figure 3: Experiment results on three testing images in the hyperspectral database [3]. The spectral distributions for three randomly selected pixels from each test image are shown in every column.

average NRMSD of our method is 4.42% on the NikonD90 and 3.94% on the Olympus EPL2. To further demonstrate the robustness against swapping camera response functions, we also train the model with one camera and then reconstruct the hyperspectral data from RGB images simulated by another camera from the dataset [3]. We find the performance between some pairs from the same camera manufacturer, such as Canon20D and Canon5D Mark II, is still reasonable, with an average NRMSD of 7.87%. However, for the pair between different manufacturers such as Canon1D Mark III and Nikon D90, it will deteriorate to 13.9%.

#### 4.4. Real Images

We also use a commercial Nikon D4S camera to capture some images of outdoor scenes (see Fig. 6 (a,b) for examples). To alleviate the influence of camera nonlinear

intensity response and unexpected image compression, we use instead the RAW files and convert them into RGB images. The camera spectral response function is provided by the sensor maker. For this specific response function, we learn a nonlinear mapping again by using the aforementioned training set, and use it to recover spectra from RGB values. Fig. 6(c) show the recovered spectra for the four color patches from our method, [23] and [3]. We can see that our method works better than the others, which verifies again the benefits in accounting for the intrinsic dimensions of natural spectra. We also note that, compared with the synthetic experiments, the performance of three methods slightly degrades. This might be attributed to the error in the camera spectral response function.

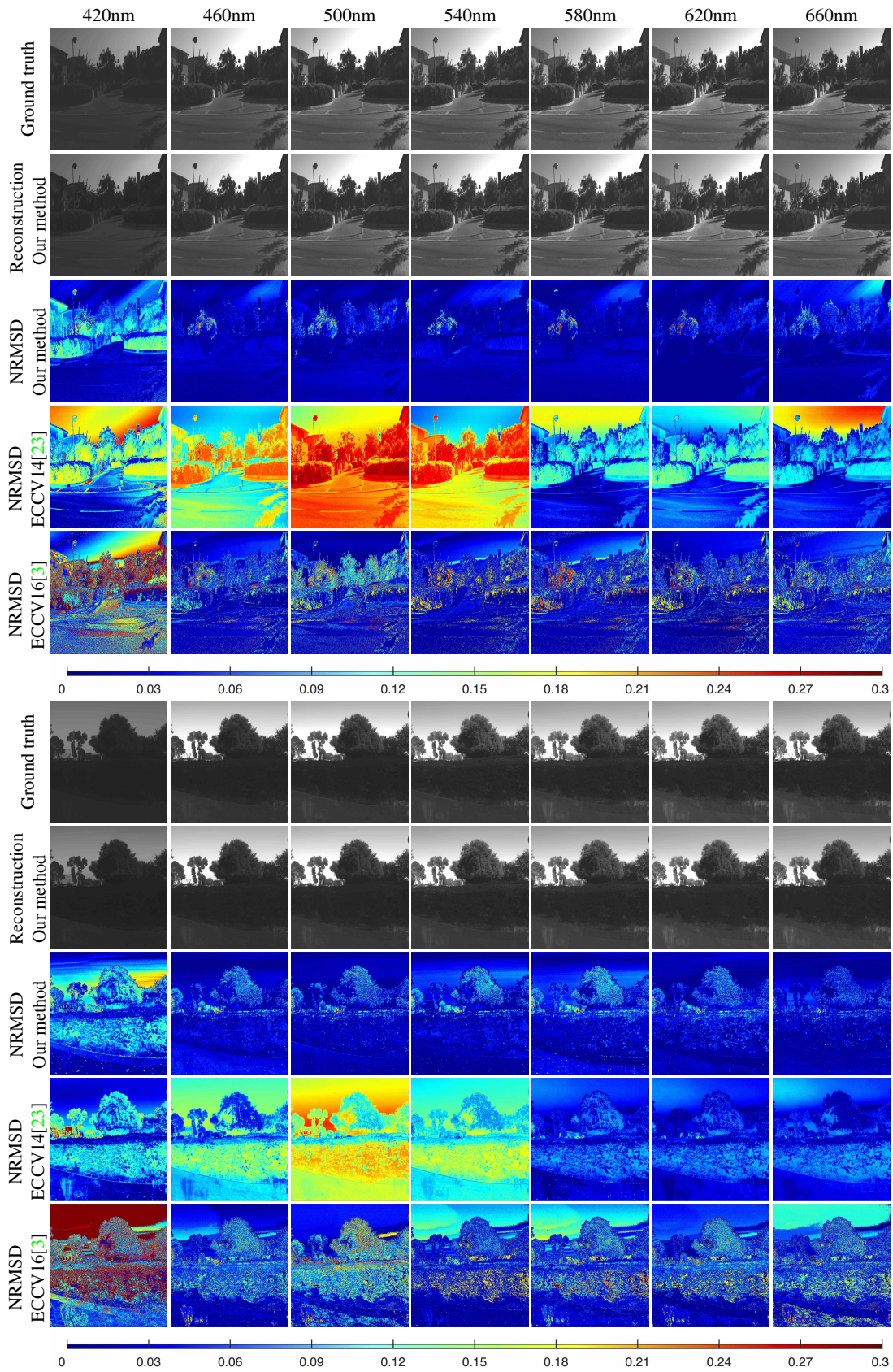


Figure 4: Sample results from the hyperspectral database [3].

Best Performance						
NRMSD						
Our	2.02%	2.52%	2.54%	2.69%	2.78%	
[23]	19.06%	11.79%	18.78%	13.08%	17.84%	
[3]	3.81%	6.22%	3.70%	5.29%	6.30%	
Worst Performance						
NRMSD						
Our	8.74%	7.30%	7.25%	6.28%	6.16%	
[23]	19.73%	13.42%	44.06%	21.18%	12.61%	
[3]	9.16%	8.22%	14.08%	9.51%	6.97%	

Figure 5: The scenarios where our method works best and worst. The comparison of corresponding average NRMSD is also provided.

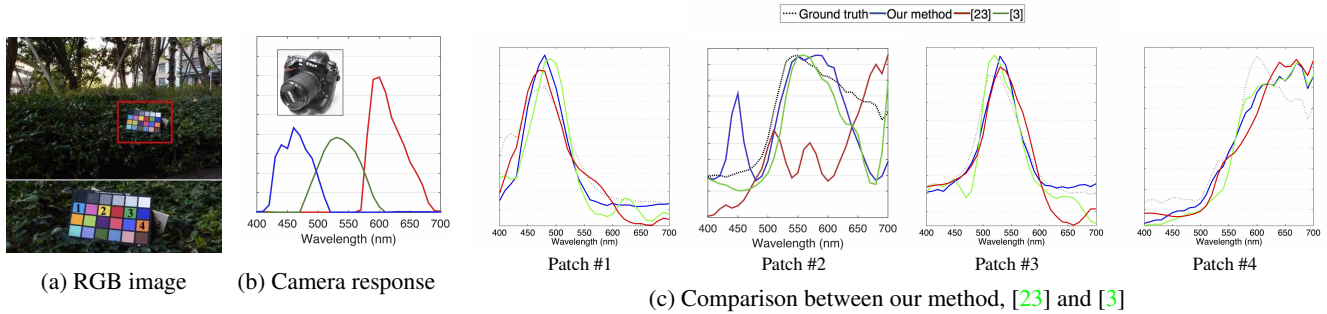


Figure 6: Experiment results of real-world scenario using a commercial Nikon D4S camera. (a) The RGB image of the scene with a color checker board. (b) The camera spectral response function provided by the maker. (c) Recovered spectra from our method, [23] and [3] for the four color patches indicated in (a).

## 5. Conclusion

We have explored the intrinsic dimensionality of the spectral space of natural scenes and found that a low dimensional embedding by Isomap is enough, to a large extent, to account for the spectral variance. This has allowed us to train a neural network based nonlinear mapping between the RGB color space and the three-dimensional embedding, by using only a small amount of representative data in an efficient manner. Experiments using synthetic images and real world data have verified the effectiveness of our nonlinear mapping based method for spectral super-resolution, as well as its advantages over existing approaches.

In this paper, we have concentrated primarily on the

spectra of natural scenes, which is relevant to consumer RGB device based spectral imaging of outdoor objects under daylight illumination. The illumination spectra for indoor illuminants are more complex. An extensive evaluation of our spectral recovery method for indoor scenes deserves to be conducted in our future work.

## Acknowledgement

The majority of this paper was finished when Yan Jia was visiting National Institute of Informatics (NII), Japan, funded by the NII MOU Internship Program. This work was supported in part by JSPS KAKENHI Grant Number JP15H05918 and JP16K16095.

## References

- [1] N. Akhtar, F. Shafait, and A. Mian. Hierarchical beta process with gaussian process prior for hyperspectral image super resolution. In *Proc. of European Conference on Computer Vision (ECCV)*, pages 103–120, Oct. 2016. 2
- [2] R. K. Antonio. Single image spectral reconstruction for multimedia applications. In *the 23rd ACM International Conference on Multimedia*, pages 251–260, 2015. 1, 3
- [3] B. Arad and O. Ben-Shahar. Sparse recovery of hyperspectral signal from natural rgb images. In *Proc. of European Conference on Computer Vision (ECCV)*, pages 19–214, Oct. 2016. 1, 3, 4, 5, 6, 7, 8
- [4] F. Ayala, J. F. Echávarri, P. Renet, and A. I. Negueruela. Use of three tristimulus values from surface reflectance spectra to calculate the principal components to reconstruct these spectra by using only three eigenvector. *Journal of the Optical Society of America A*, 23(8):2020–2026, Sep. 2006. 2, 3
- [5] X. Cao, H. Du, X. Tong, Q. Dai, and S. Lin. A Prism-Mask System for Multispectral Video Acquisition. *IEEE Trans. Pattern Analysis and Machine Intelligence (PAMI)*, 33(12):2423–2435, 2011. 2
- [6] X. Cao, X. Tong, Q. Dai, and S. Lin. High resolution multispectral video capture with a hybrid camera system. In *Proc. of IEEE Conference on Computer Vision and Pattern Recognition (CVPR)*, pages 297–304, 2011. 2
- [7] A. Chakrabarti and T. Zickler. Statistics of real-world hyperspectral images. In *Proc. of IEEE Conference on Computer Vision and Pattern Recognition (CVPR)*, pages 193–200, June 2011. 4, 5
- [8] C. Chi, H. Yoo, and M. Ben-Ezra. Multi-Spectral Imaging by Optimized Wide Band Illumination. *International Journal of Computer Vision (IJCV)*, 86(2-3):140–151, 2010. 2
- [9] J. Cohen. Dependency of the spectral curves of the munsell color chips. *Psychonomic science*, 1(1-12):369–370, Jan. 1964. 2, 3
- [10] M. Descour and E. Dereniak. Computed tomography imaging spectrometer: Experimental calibration and reconstruction results. *Applied Optics*, 34(22):4817–4826, 1995. 2
- [11] M. Donald. An algorithm for least-squares estimation of nonlinear parameters. *SIAM Journal on Applied Mathematics*, 11(2):431–441, 1963. 4
- [12] Y. Fu, Y. Zheng, I. Sato, and Y. Sato. Exploiting spectral-spatial correlation for coded hyperspectral image restoration. In *Proc. of IEEE Conference on Computer Vision and Pattern Recognition (CVPR)*, pages 3727–3736, 2016. 2
- [13] L. Gao, R. Kester, N. Hagen, and T. Tomasz. Snapshot image mapping spectrometer (IMS) with high sampling density for hyperspectral microscopy. *Optical Express*, 18(14):14330–14344, 2010. 2
- [14] N. Gat. Imaging spectroscopy using tunable filters: a review. In *Proc. of SPIE, Wavelet Applications VII*, volume 4056, pages 50–64, 2000. 2
- [15] S. Han, I. Sato, T. Okabe, and Y. Sato. Fast Spectral Reflectance Recovery Using DLP Projector. *International Journal of Computer Vision (IJCV)*, pages 1–13, Dec. 2013. 2
- [16] T. Jaaskelainen, J. Parkkinen, and S. Toyooka. Vector-subspace model for color representation. *Journal of the Optical Society of America A*, 7(4):725–730, 1990. 2, 3
- [17] R. Kawakami, J. Wright, Y.-W. Tai, Y. Matsushita, M. Ben-Ezra, and K. Ikeuchi. High-resolution hyperspectral imaging via matrix factorization. In *Proc. of IEEE Conference on Computer Vision and Pattern Recognition (CVPR)*, pages 2329–2336, 2011. 2
- [18] L. Kenneth. A method for the solution of certain non-linear problems in least squares. *Quarterly of Applied Mathematics*, 2:164–168, 1944. 4
- [19] A. Lam, A. Subpa-Asa, I. Sato, T. Okabe, and Y. Sato. Spectral imaging using basis lights. In *Proceedings of the British Machine Vision Conference*. BMVA Press, 2013. 2
- [20] J. MacQueen. Some methods for classification and analysis of multivariate observations. In *Proceedings of the fifth Berkeley symposium on mathematical statistics and probability.*, volume 1, pages 281–297, California, USA, 1967. 5
- [21] L. T. Maloney. Evaluation of linear models of surface spectral reflectance with small numbers of parameters. *Journal of the Optical Society of America A*, 3(10):1673–1683, Nov. 1986. 2, 3
- [22] D. H. Marimont and B. A. Wandell. Linear models of surface and illuminant spectra. *Journal of the Optical Society of America A*, 9(11):1905–1913, 1992. 2, 3
- [23] R. M. H. Nguyen, D. K. Prasad, and M. S. Brown. Training-Based Spectral Reconstruction from a Single RGB Image. In *Proc. of European Conference on Computer Vision (ECCV)*, pages 186–201, Sept. 2014. 1, 3, 5, 6, 7, 8
- [24] J.-I. Park, M.-H. Lee, M. D. Grossberg, and S. K. Nayar. Multispectral Imaging Using Multiplexed Illumination. In *Proc. of International Conference on Computer Vision (ICCV)*, pages 1–8, 2007. 2
- [25] J. P. S. Parkkinen, J. Hallikainen, and T. Jaaskelainen. Characteristic spectra of munsell colors. *Journal of the Optical Society of America A*, 6(2):318–322, 1989. 2, 3
- [26] J. B. Tenenbaum, V. de Silva, and J. C. Langford. A global geometric framework for nonlinear dimensionality reduction. *Science*, 290:2319–2323, 2000. 3, 4
- [27] A. Wagadarikar, N. Pitsianis, X. Sun, and B. David. Video rate spectral imaging using a coded aperture snapshot spectral imager. *Optical Express*, 17(8):6368–6388, 2009. 2
- [28] F. Yasuma, T. Mitsunaga, D. Iso, and S. Nayar. Generalized assorted pixel camera: Post-capture control of resolution, dynamic range and spectrum. Technical report, Nov. 2008. 4, 5
- [29] Z. Zhao and G. Feng. A dictionary-based algorithm for dimensionality reduction and data reconstruction. In *22nd International Conference on Pattern Recognition (ICPR)*, pages 1556–1561. IEEE, Dec. 2014. 4